Available online at www.sciencedirect.com
ScienceDirect
Trans. Nonferrous Met. Soc. China 35(2025) 625−639
Transactions of Nonferrous Metals Society of China
www.tnmsc.cn

Formation mechanism of bonded slag pellets in vertical-pot Pidgeon process of magnesium production

Ji-lei XU[1], Jin-hui LIU[1], Yu-ming ZHAO[2], Zhi-ping MAO[1], Wei-neng TANG[3], Xiao-feng LI[3], Pei-xu YANG[1], Wei-dong ZHANG[1], Shao-jun ZHANG[1]

1. School of Materials Science and Engineering, Zhengzhou University, Zhengzhou 450001, China;
2. College of Materials Engineering, Henan University of Engineering, Zhengzhou 451191, China;
3. Baosteel Metal Co., Ltd., China Baowu Steel Group Corporation, Shanghai 200940, China

Received 6 June 2023; accepted 27 February 2024

Abstract: In the Pidgeon process involving a vertical pot, bonded slag pellets occasionally emerge at the bottom of the reduction pot, impeding smooth slag discharge. To reveal the formation mechanism of the bonded slag pellets, thermodynamic calculations, X-ray diffraction (XRD), X-ray fluorescence spectrometry (XRF), electron probe microanalyzer (EPMA), X-ray photoelectron spectroscopy (XPS), and differential scanning calorimetry (DSC) were employed. The bonded slag pellets mainly comprise MgO, $CaSi_2$, CaO, and Ca_2SiO_4. $CaSi_2$ in the bonded slag pellets is attributed to the reduction reaction between Si and CaO, yielding liquid $CaSi_2$. Simultaneously, the reaction between $CaSi_2$ and MgO, which will typically produce Mg vapor, is inhibited, resulting in the accumulation of $CaSi_2$. Owing to the solid–liquid transition of $CaSi_2$, this process culminates in the bonding of slag pellets. This study can guide the Pidgeon process optimization, enabling mitigation of the "dead pot" issue, thereby enhancing efficiency and reducing costs.

Key words: vertical-pot Pidgeon process; slag discharge; bonded slag pellets; $CaSi_2$; solid−liquid transition

1 Introduction

Magnesium and its alloys exhibit immense potential in automotive, electronic, and biomedicine applications [1−3] owing to their several advantages such as low density, high specific strength and specific stiffness [4−6], effective thermal and magnetic shielding, excellent damping capacity and electrical conductivity [7,8], and superior biocompatibility.

Generally, magnesium production primarily involves electrolysis and thermal reduction. The Pidgeon process, a thermal reduction method, utilizes ferrosilicon as the reducing agent to extract magnesium from dolime under vacuum conditions [9]. This process has gained rapid development in China owing to its simplicity, low equipment investment, high-purity output, and alignment with the mineral and energy conditions pertinent to China. In recent years, the primary magnesium output using the Pidgeon process in China accounts for more than 70% of the global total magnesium production [10−12].

The traditional horizontal-pot Pidgeon process involves manual feeding and slag discharge under high temperature conditions, and it encounters challenges such as low mechanical efficiency, high labor intensity, and harsh operating conditions [13−15]. On the contrary, the vertical-pot Pidgeon process can realize automatic charging and discharging by leveraging the gravity of pellets

Corresponding author: Jin-hui LIU, Tel: +86-13592583686, E-mail: liujinhui@zzu.edu.cn
DOI: https://doi.org/10.1016/S1003-6326(24)66704-X

and reduced slag, which considerably reduces the labor intensity, enhances the working environment, and improves the production efficiency. Recent experimental research on the application of external-heating vertical pots in the Pidgeon process has led to its adoption in certain areas for primary magnesium production [16]. However, during practical operations, the vertical-pot process encounters operational challenges, especially in slag discharge. These issues primarily arise from two phenomena: (1) slag pellets adhering to the reduction pot wall and (2) slag pellets bonding at the bottom of the vertical pot during the reduction process.

The mechanism underlying the adhesion of slag pellets to the reduction pot wall during magnesium production has been investigated, revealing that Al_2O_3 and CaF_2 play an important role in the glaze formation. The solid–liquid transition of this glaze triggers the sticking of slag pellets to the pot wall [17]. In the case of the slag pellets bonding at the bottom of the vertical pot during the reduction process, the bonded pellets exhibit considerable strength and hardness, complicating their breakage and impeding slag discharge. This phenomenon is commonly referred to as “dead pot” in the industry, and its formation mechanism remains unclear.

Despite several studies, the chemical reaction pathway in the silicon thermal reduction of dolime is a subject of ongoing debate [18−20]. This reaction process entails two prevailing perspectives: the first suggests a direct reaction between the reducing agent Si and CaO·MgO, without intermediate products, as outlined in Reaction (1) [13,21]:

$$Si(s)+2CaO\cdot MgO(s)=2Mg(g)+Ca_2SiO_4(s) \quad (1)$$

The second view posits the initial formation of the intermediate compound silicocalcium (CaSi or $CaSi_2$), which subsequently participates in the reduction reaction, as detailed in Reactions (2)−(5) [22−24]:

$$5Si(s)+4CaO(s)=2CaSi_2(l)+Ca_2SiO_4(s) \quad (2)$$

$$3Si(s)+4CaO(s)=2CaSi(s)+Ca_2SiO_4(s) \quad (3)$$

$$2MgO(s)+2/5CaSi_2(l)+6/5CaO(s)=2Mg(g)+4/5Ca_2SiO_4(s) \quad (4)$$

$$2MgO(s)+2/3CaSi(s)+2/3CaO(s)=2Mg(g)+2/3Ca_2SiO_4(s) \quad (5)$$

This study explores the formation mechanism of bonded slag pellets at the bottom of the reduction pot in magnesium production using the vertical-pot Pidgeon process. This investigation aims to facilitate the automation and mechanization of magnesium production using the Pidgeon process. The study establishes a causal link between the formation of intermediate silicocalcium compounds and the occurrence of bonded slag pellets.

2 Experimental

2.1 Materials

The raw materials for preparing pellets included dolomite ($CaCO_3\cdot MgCO_3$), 75% ferro-silicon alloy (FeSi75), and fluorite (CaF_2). The chemical composition of dolomite was determined using an ICP-OES analyzer (iCAP 7200, Thermo Scientific, America), as depicted in Table 1. The ferrosilicon alloy adopted the certified reference material standards, and its chemical composition is listed in Table 2.

Table 1 Composition and calcining index of dolomite (wt.%)

MgO	CaO	Al_2O_3	Fe_2O_3	K_2O	Others	CO_2
22.31	31.22	0.05	0.05	0.02	0.82	47.02

Table 2 Chemical composition of ferrosilicon alloy (wt.%)

Si	Fe	Al	Others
77.6	19.3	1.24	4.86

The dolime (CaO·MgO) was in accordance molar ratio of CaO/MgO about 1. Dolomite was crushed into particles size of about 5 mm to calcine at 1100 °C for 1.5 h. Subsequently, the calcined dolime was sieved through a 75 μm sieve. To elucidate the challenges associated with slag discharge in the vertical-pot Pidgeon process, the bonded pellets were sourced from actual production.

These pellets were provided by the demonstration production line of magnesium at the compound vertical pot of Zhengzhou University, China. The bonded pellets were retrieved by manually removing the reduction slag from the bottom of the reduction pots, where difficulties in slag discharge were encountered.

2.2 Thermodynamic calculations

The aim of this study was to analyze the

potential composition, physicochemical properties, and thermodynamic equilibrium phases of pellets during the magnesium production. It involved calculating the potential reactions in the pellets, their initial melting temperatures, and phase content using Factsage 8.2, with FactPS and FToxid as the selected databases. The Gibbs free energy change under standard conditions was calculated using Eq. (6):

$$\Delta G_T^{\Theta} = \Delta H_T^{\Theta} - T\Delta S_T^{\Theta} \tag{6}$$

where ΔG_T^{Θ} represents the change in Gibbs free energy of the chemical reaction at standard pressure, T denotes the chemical reaction temperature, ΔH_T^{Θ} indicates the variation in enthalpy of the chemical reaction, and ΔS_T^{Θ} denotes the entropy variation of the chemical reaction. The temperature and pressure relations for the reaction were determined by setting ideal reaction conditions and utilizing the thermodynamic database.

2.3 Preparation of sample

First, dolime, ferrosilicon alloy, and fluorite were uniformly mixed according to a certain proportion by ball milling in a planetary mill at 200 r/min for 0.5 h. The raw material of the pellets was proportioned according to the rule that the molar ratio of Si/MgO was 0.5 and the mass fraction of fluorite was 3%. Then, the obtained powder mixture was placed into the mold with an inner diameter of 25 mm and shaped into pellets at a pressure of 150 MPa. The obtained pellets were stacked together to observe whether bonding phenomenon occurred. Finally, the pellets were placed in an alumina crucible and sintered using a tubular high temperature furnace (GSL−1700X, Kejing, China).

In the comparative experiments, argon gas was first used to purge the air from the furnace. The vacuum reactor was heated to the specified temperature at a heating rate of 10 K/min, and the vacuum state was consistent with the set state during the experiment. The process initially involved reducing the reactor pressure to below 1 Pa using a vacuum pump, followed by filling the reactor with argon gas to achieve the target pressure. The pressure was then stabilized at the desired value by adjusting the valve angle, which was monitored by a custom-modified pressure gauge.

According to the change of mass loss in the pellets before and after the reaction, the conversion rate of magnesium was evaluated using Eq. (7):

$$\eta = \frac{m_{\text{before}} - m_{\text{after}}}{m_{\text{before}} w} \times 100\% \tag{7}$$

where η denotes the conversion rate of pellets, w is the magnesium mass fraction in the pellets, and m_{before} represents the mass of the pellets before the reduction reaction, and m_{after} denotes the mass after the reduction reaction.

2.4 Microstructural characterization

A thermogravimetric analyzer with differential scanning calorimetry (TG−DSC, STA 449F3, Netzsch, Germany) was used to measure the liquid-phase temperature and reaction characteristics of the bonded pellets. An X-ray diffraction spectrometer (XRD, XRD6100, SHIMADZU, Japan) and an X-ray photoelectron spectroscope (XPS, Thermo ESCALAB 250XI) were used to analyze the composition and main phase of the pellets. The precise elemental contents in the bonded pellets were determined using an X-ray fluorescence spectrometer (XRF, ARL PERFORM'X 4200W, Thermo Fisher Scientific, USA).

The polished cross-sections of the samples, embedded in epoxy resin, were examined through scanning electron microscope (SEM, Helios G4 CX, Thermo Fisher Scientific, USA) at an accelerating voltage of 20 kV in the backscattered electron mode (BSE). Energy dispersive spectroscopy (EDS) was used to measure the chemical composition of the specimen and ascertain the distribution of elements. A more accurate analysis of the elemental distribution was obtained using a field emission electron probe microanalyzer (EPMA, EPMA−8050G, SHIMADZU, Japan).

3 Results and discussion

3.1 Macromorphology of bonded slag pellets

In the vertical pot, pellets are predominantly accumulated between the pot wall and the center cylinder, as depicted in Fig. 1(a). The central cylinder plays a role in transporting Mg vapor to the crystallizer, regulating the pellet layer thickness, facilitating slag discharge, and other applications. For instance, after the termination of the reduction

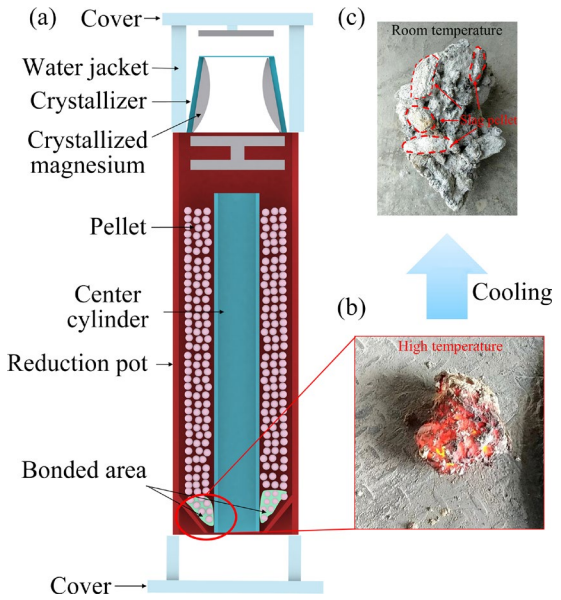

Fig. 1 Schematic diagram (a) and morphologies (b, c) of bonded slag pellets at bottom of reduction pot during magnesium production in vertical-pot Pidgeon process

process, the central cylinder is lifted, and under gravity, the slag pellets fall from the bottom of the reduction pot. Nevertheless, bonded slag pellets are occasionally formed at the base of the pot, exhibiting considerable strength and hardness that they cannot be disintegrated easily, as illustrated in Figs. 1(a) and (b). This occurrence of bonded slag pellets impedes automatic slag discharge, a phenomenon referred to as “dead pot”. The morphologies of these bonded slag pellets at high temperature and room temperature are displayed in Figs. 1(b) and (c), respectively.

Typically, the slag pellets from the Pidgeon process experience pulverization during cooling owing to the crystal transition from β-Ca_2SiO_4 to γ-Ca_2SiO_4 [25]. However, these bonded, hard slag pellets maintain their shape and compactness during cooling, as depicted in Fig. 1(c), and continue to exhibit high strength and hardness at room temperature.

3.2 Chemical composition and phase consitution of bonded slag pellets

Table 3 presents the chemical compositions of the bonded slag pellets and the initial pellets, which are a mixture of calcined dolomite, ferrosilicon, and fluorite. XRF analysis reveals that the Mg contents in the bonded slag pellets and the initial pellets are 17.24 and 20.72 wt.%, respectively, indicating only 16.8% conversion of Mg. The contents of other elements in the two samples are comparatively similar.

The XRD patterns of the bonded slag pellets and those subjected to specific treatments are presented in Fig. 2. The bonded slag pellets display the pronounced peaks of β-Ca_2SiO_4, MgO, $CaSi_2$ [26−28], and CaO, without peaks of γ-Ca_2SiO_4. The phase transitions between various crystalline forms of Ca_2SiO_4 can spontaneously occur with a change in temperature. For instance, the $\beta \rightarrow \gamma$ transition involves an irreversible reconstructive phase change, accompanied by a significant volume increase that causes the pulverization of magnesium slag upon cooling. However, intriguingly, the crystal transition from β-Ca_2SiO_4 to γ-Ca_2SiO_4 does not occur in the bonded slag pellets, explaining the absence of natural pulverization in these pellets.

The presence of prominent peaks of MgO in the bonded slag pellets indicates incomplete completion of the reduction reaction, which is consistent with XRF results. On the other hand, it can be observed that the peak intensity of MgO in the bonded slag pellets is higher than that of CaO. This contrasts with their intensities in the pattern of the initial pellets, where the peak intensity of CaO is higher than that of MgO. This indicates that the actual consumption of CaO is much greater than that of MgO during the reactions. The distinct $CaSi_2$ peak in the bonded slag pellets, coupled with reports from prior studies [22,24], confirms that Reaction (2) occurs and generates silicocalcium as an intermediate product. This accounts for the absence of Si peaks in the bonded slag pellet pattern.

Table 3 Chemical compositions of bonded and initial pellets

Sample	Content/wt.%						
	Mg	Ca	Si	Fe	CaF_2	Al_2O_3	Other
Bonded slag pellets	17.24	33.25	13.89	3.42	1.1	1.59	–
Initial pellets	20.72	34.12	13.21	3.61	1.8	0.98	–

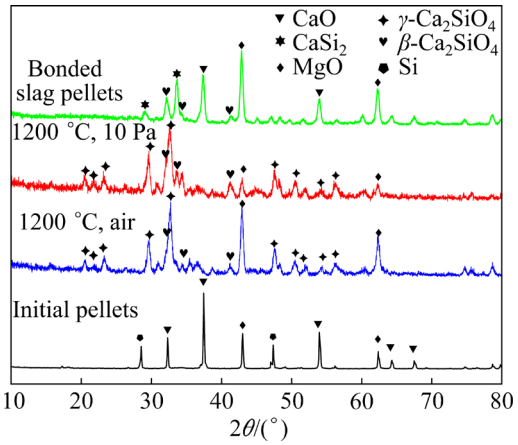

Fig. 2 XRD patterns of bonded slag pellets and those after treatment under 1200 °C, 10 Pa and 1200 °C, air conditions

Subsequently, the bonded slag pellets were heated to 1200 °C and held for 2 h under vacuum (~10 Pa). The pattern revealed a substantial weakening in the diffraction peaks of MgO, CaO, and $CaSi_2$, combined with the strong peaks of γ-Ca_2SiO_4, indicating that Reaction (4) occurs under these conditions.

Another treatment of the bonded slag pellets was heated to 1200 °C and held for 2 h under air atmosphere. Although the intensity of the diffraction peaks of $CaSi_2$ and CaO considerably weakened, the intensity of the MgO peak remained largely unchanged, suggesting that $CaSi_2$ did not reduce MgO but instead oxidized directly to form Ca_2SiO_4 in the presence of oxygen, as per Reaction (8). The slag obtained from these two treatments underwent pulverization because of the crystal transition from β-Ca_2SiO_4 to γ-Ca_2SiO_4.

$$CaSi_2(l)+5/2O_2(g)+3CaO(s)=2Ca_2SiO_4(s) \quad (8)$$

To verify the presence of $CaSi_2$, the chemical states of Mg, Si, and Ca in the bonded slag pellets were examined using XPS, as depicted in Fig. 3. The broad spectra in Fig. 3(a) reveal that the primary elements in the bonded slag pellets and those treated at 1200 °C in air include Ca, O, Mg, and Si, with trace amounts of Fe and F. However,

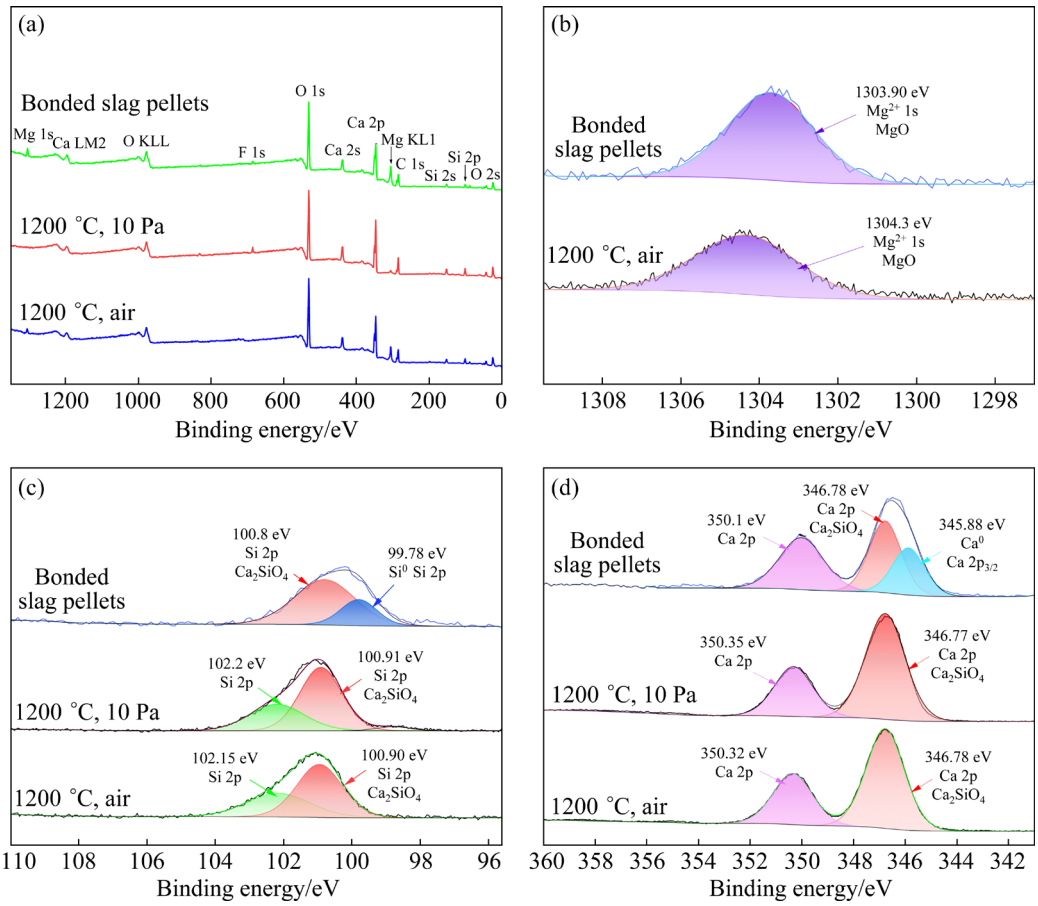

Fig. 3 XPS analysis results of bonded slag pellets and those after treatment under different conditions: (a) Wide spectra; (b) Mg 1s; (c) Si 2p; (d) Ca 2p

the peaks of the Mg element of the residue after treatment at 1200 °C and 10 Pa are virtually absent, which are consistent with the XRF and XRD results. Figure 3(b) illustrates the Mg 1s orbital characteristic peaks of the bonded slag pellets and their air-treated counterparts at 1200 °C. The peaks observed at binding energies of 1303.9 and 1304.5 eV correspond to MgO.

The Si 2p orbitals of the bonded slag pellets and those after treatment under conditions of 1200 °C, 10 Pa and 1200 °C, air are portrayed in Fig. 3(c). In these three samples, the peaks with binding energies of 100.80, 100.91, and 100.90 eV are attributed to Ca_2SiO_4 [29]. In the bonded slag pellets, a peak with a binding energy of 99.78 eV belongs to Si^0 [30,31]. Two main peaks with binding energies of 102.2 and 102.15 eV, which belong to calcium silicate hydrate produced by the reaction with atmospheric water and carbon dioxide, are observed in the bonded pellets after treatments under conditions of 1200 °C, 10 Pa and 1200 °C, air [32].

Figure 3(d) shows the characteristic peaks of the Ca 2p orbitals of the bonded slag pellets and those after treatment under conditions of 1200 °C, 10 Pa and 1200 °C, air. In these three samples, the binding energy peaks with binding energies of 346.77 and 346.78 eV belong to Ca_2SiO_4. Two main peaks with binding energies of 345.88 and 350.01 eV can be observed in bonded slag pellets, representing Ca^0 and CaO, respectively [33]. The concurrent presence of Si^0 and Ca^0 in the bonded pellets and their disappearance after treatment under conditions of 1200 °C, 10 Pa and 1200 °C, air signify the existence of silicocalcium in the bonded slag pellets. These results imply that the pellets underwent Reaction (2) at the bottom of the reduction pot, producing Ca_2SiO_4 and $CaSi_2$, whereas Reaction (4) was impeded by specific factors, which is consistent with the analysis results of the XRF and XRD.

3.3 Thermodynamic analysis results

The Gibbs free energy change (ΔG) of silicocalcium formation in the CaO−Si system was calculated versus temperature according to the Factsage 8.2 Reaction module, and the results are shown in Fig. 4(a). The results indicate that $CaSi_2$ and CaSi can be produced within the temperature interval of magnesium production by the Pidgeon process, while Ca_2Si cannot be formed. Notably, the maximum ΔG value is observed for the formation of $CaSi_2$. These findings suggest that the formation of $CaSi_2$ is most likely to occur at the early stage of silicocalcium formation in the CaO−Si system, despite a CaO/Si molar ratio of 2.0 in the pellets.

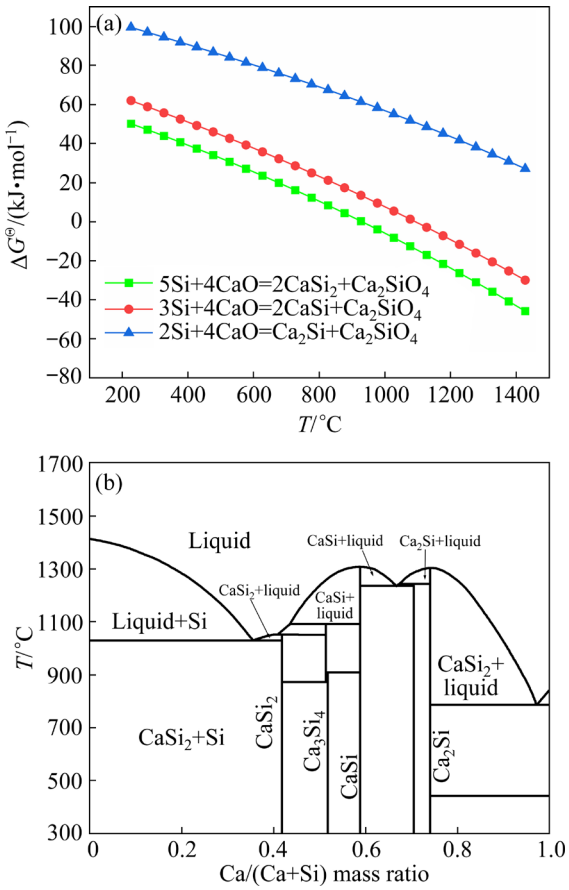

Fig. 4 $\Delta G^{\ominus}$−T diagrams of reactions of CaO−Si system (a) and binary phase diagram of Ca−Si system at 1.013×10^5 Pa (b)

The binary phase diagram of Ca−Si system is shown in Fig. 4(b). The analysis of this diagram can be used to determine whether the Ca−Si system produces a liquid phase during the Pidgeon process. The Ca−Si binary alloy primarily comprises three stable intermediate phases: $CaSi_2$, CaSi, and Ca_2Si [28]; the lowest temperatures at which these phases convert to a liquid state involve 1050, 1307, and 1302 °C, respectively. In the presence of silicon, the minimum temperature required for the formation of a liquid-phase region in $CaSi_2$ is 1028 °C.

Thermogravimetric (TG) and DSC tests were conducted to evaluate the thermochemical properties of the bonded slag pellets, including

those subjected to treatment at 1200 °C under 10 Pa and in air. The assessments were performed in an Ar atmosphere, with a heating ramp rate of 10 °C/min, ranging from 50 to 1200 °C. The results are shown in Fig. 5. In Fig. 5(b), the DSC curve of the bonded slag pellets exhibits a distinct heat absorption peak at 1026 °C, whereas the TG curve displays no mass loss at this temperature (Fig. 5(a)). On the contrary, the DSC curves of the post-treatment bonded pellets under conditions of 1200 °C, 10 Pa and 1200 °C, air reveal no heat absorption peaks throughout the entire temperature range.

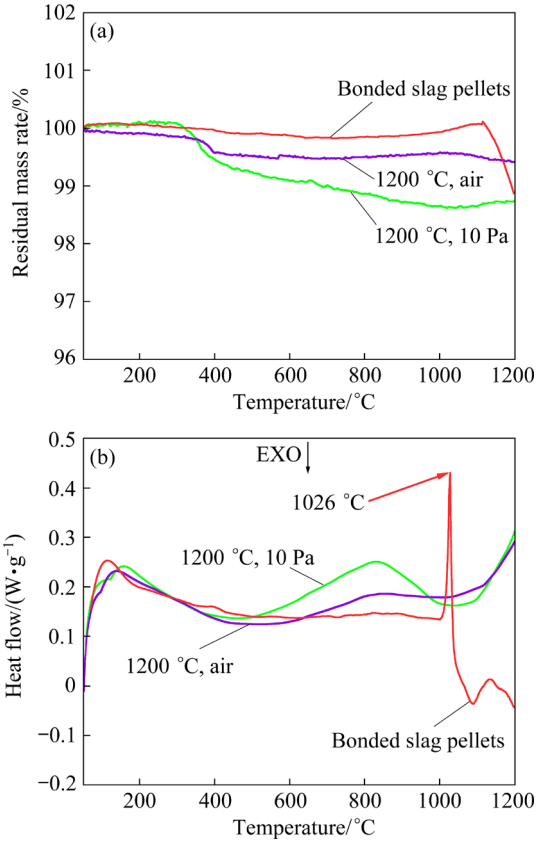

Fig. 5 TG (a) and DSC (b) curves of bonded slag pellets and those after treatment under conditions of 1200 °C, 10 Pa and 1200 °C, air

Coupled with the XRD analysis results indicating the absence of Si in the bonded slag pellets, it can be deduced that the observed heat absorption peak is not associated with a chemical reaction but linked to a solid−liquid transition. Based on both Gibbs free energy changes of the CaO−Si system as a function of reaction temperature (Fig. 4(a)) and the binary phase diagram of the Ca−Si system (Fig. 4(b)), the solid−liquid transition likely corresponds to the formation of $CaSi_2$, thereby substantiating its presence.

The relationship between the initial reaction temperature and the equilibrium pressure of Reaction (4) is plotted in Fig. 6, as derived from the calculated results. In this system, the system pressure is equal to the magnesium vapor pressure. The initial reaction temperature gradually increases with rising system pressure. When the actual system pressure surpasses the equilibrium pressure, Reaction (4) is hindered. Under such conditions, only Reaction (2) will occur, resulting in the preservation of $CaSi_2$ as a product, without its subsequent consumption.

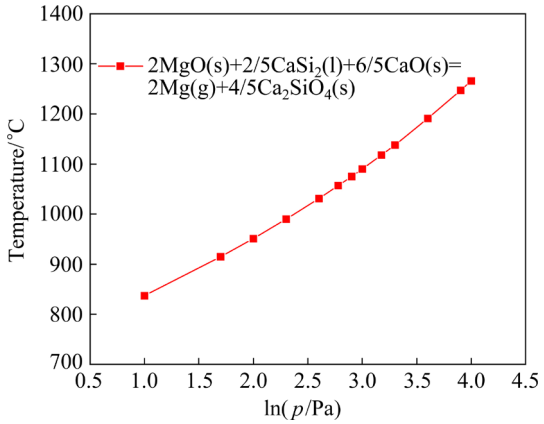

Fig. 6 Relationship between initial reaction temperature and equilibrium pressures (p) of Reaction (4)

The calculated contents of thermodynamic equilibrium phases in the pellet with a CaO·MgO/Si molar ratio of 2.0 in a temperature range of 800−1200 °C under various pressures are presented in Fig. 7. The data suggest that at a system pressure of 10 Pa (Fig. 7(a)), the direct reduction of dolime by silicon at 930 °C results in the production of magnesium vapor and slag (Ca_2SiO_4). This outcome is primarily caused by the higher initial reaction temperature of Reaction (2) compared to Reaction (4); thus, the overall reaction temperature is consistent with that of Reaction (2).

As the system pressure increases, the initial reaction temperature of Reaction (4) also increases, as indicated in Fig. 6. At a system pressure of 100 Pa, as depicted in Fig. 7(b), Si in the pellets first reduces CaO to produce solid-phase silico-calcium at 930 °C. Subsequently, this solid-phase silicocalcium reduces MgO to generate magnesium vapor and slag (Ca_2SiO_4) at 951 °C [34]. At a system pressure of 1000 Pa, the initial reaction temperature of Reaction (4) increases to 1090 °C, surpassing the

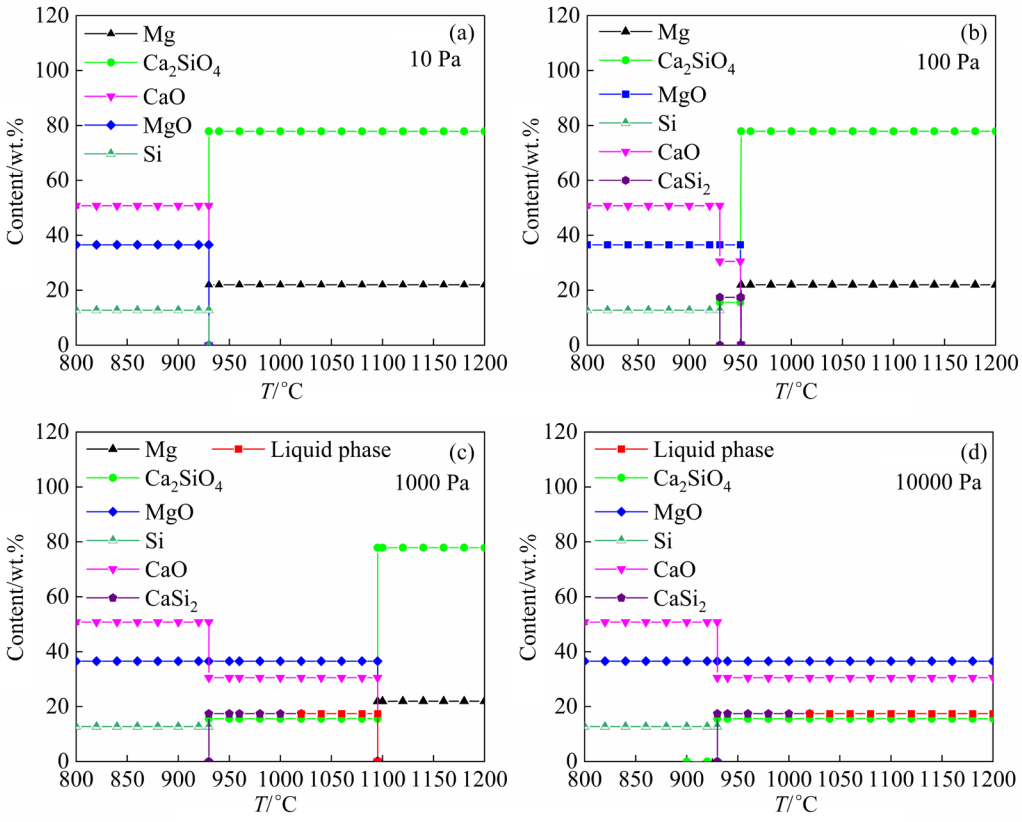

Fig. 7 Calculated contents of thermodynamic equilibrium phases of pellets under different system pressures

solid−liquid transition temperature of $CaSi_2$ (1028 °C). Thus, it can be concluded that the reducing agent in Reaction (4) is not solid $CaSi_2$ but liquid $CaSi_2$, as illustrated in Fig. 7(c). Further increasing the system pressure to 10000 Pa (Fig. 7(d)) causes the initial reaction temperature to exceed 1200 °C. Under these conditions, within the operational temperature range of the Pidgeon process, Reaction (4) will be suppressed, and the liquid $CaSi_2$ formed via Reaction (2) will remain unconsumed, as depicted in Fig. 7(d). Notably, under actual operating pressures, if the reduction temperature inside the reduction pot is lower than the initial reaction temperature of Reaction (4), the reaction will similarly be inhibited.

Based on the above analysis, the presence of MgO, CaO, $CaSi_2$, and Ca_2SiO_4 in the bonded slag pellets can be ascribed to the occurrence of Reaction (2) and the inhibition of Reaction (4) in the reduction pot under the actual conditions.

3.4 Micromorphology of bonded slag pellets

The low-magnification BSE−SEM morphology and corresponding EPMA results of the bonded slag pellets are displayed in Fig. 8. The BSE−SEM morphology reveals that most regions are smooth and crack-free after polishing, indicating a high relative density of the bonded slag pellets. The primary elemental distribution within the pellets includes Ca, Mg, O, and Si, which are consistent with the XRD and XRF results.

Notably, substantial Mg is present in the bonded slag pellets, corresponding to the gray areas observed in Fig. 8(a). The distinct separation of Mg from Ca suggests that the bonded slag pellets differ from both the pre- and post-production pellets. Additionally, the overlap of Mg and O elements indicates the distribution of MgO. Certain Ca-rich regions, overlapping with O areas having low Si content, are identified in the red zones marked as *A* in Fig. 8(e). Conversely, other Ca-rich regions coincide with O areas high in Si content, located in the yellow zones marked as *B* in Fig. 8(e). The bright spots observed in the BSE−SEM morphology correspond to areas enriched in Si and Fe, implying that these regions contain underreacted ferrosilicon particles.

The high-magnification BSE–SEM morphology and associated EPMA results of the bonded slag pellets are presented in Fig. 9. The black regions in

Fig. 9(a), enriched in Mg and O but lacking Ca and Si, denote the distribution of MgO. Excluding these black regions, the remaining areas can be divided into two distinct parts. In conjunction with the distribution of Mg, Ca, O, and Si, these two components correspond to Areas *A* and *B* identified in the low-magnification morphology.

The cross-sectional BSE−SEM morphology of the bonded slag pellets and the corresponding EDS analysis results are presented in Fig. 10. In this study, microarea chemical analyses were conducted by selecting specific points within these four regions: Points 1 and 2 in Area *A*, Point 3 in the black area, Points 4 and 5 in Area *B*, and Point 6 in

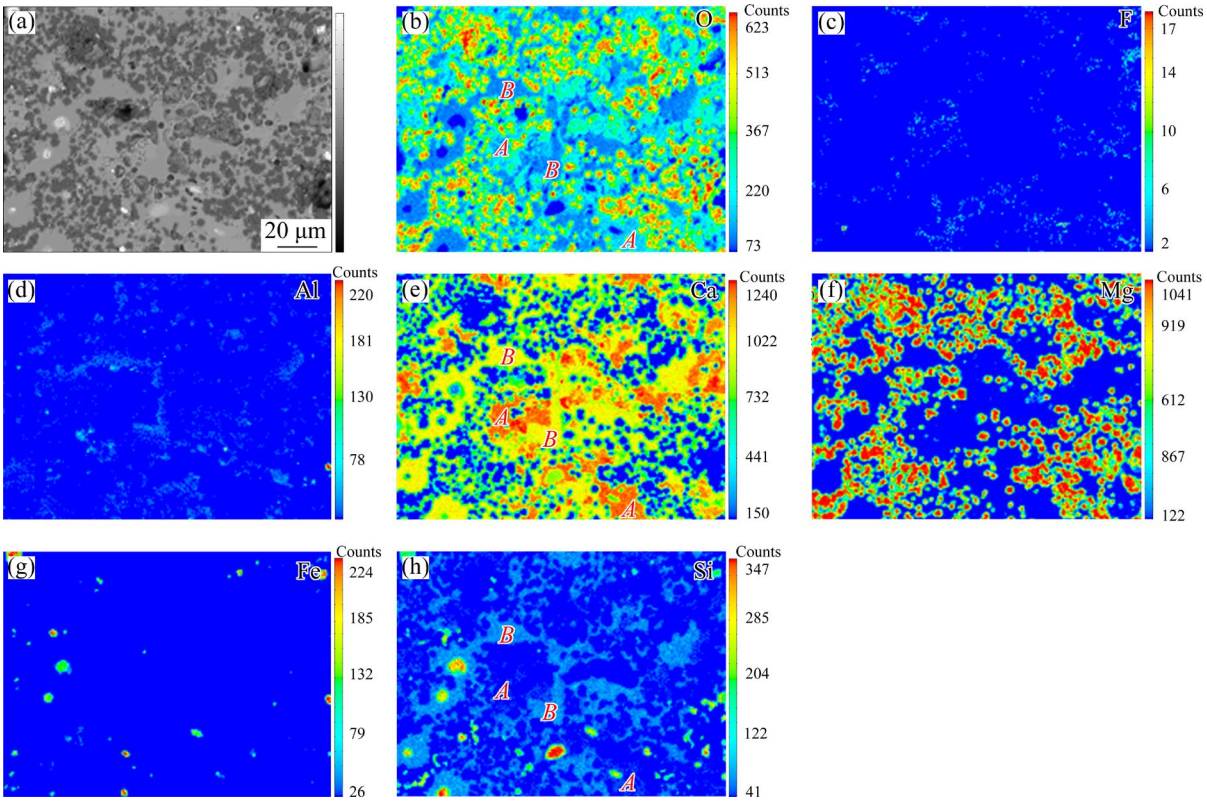

Fig. 8 Low-magnification cross-sectional BSE−SEM morphology (a) and corresponding EPMA results (b−h) of bonded slag pellets

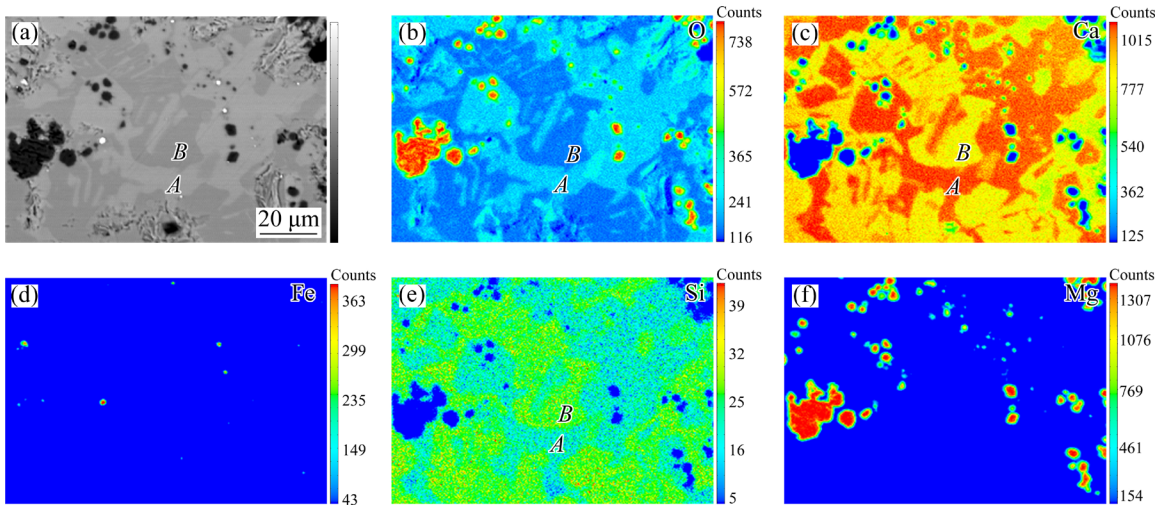

Fig. 9 High-magnification cross-sectional BSE–SEM morphology (a) and corresponding EPMA results (b−f) of bonded slag pellets

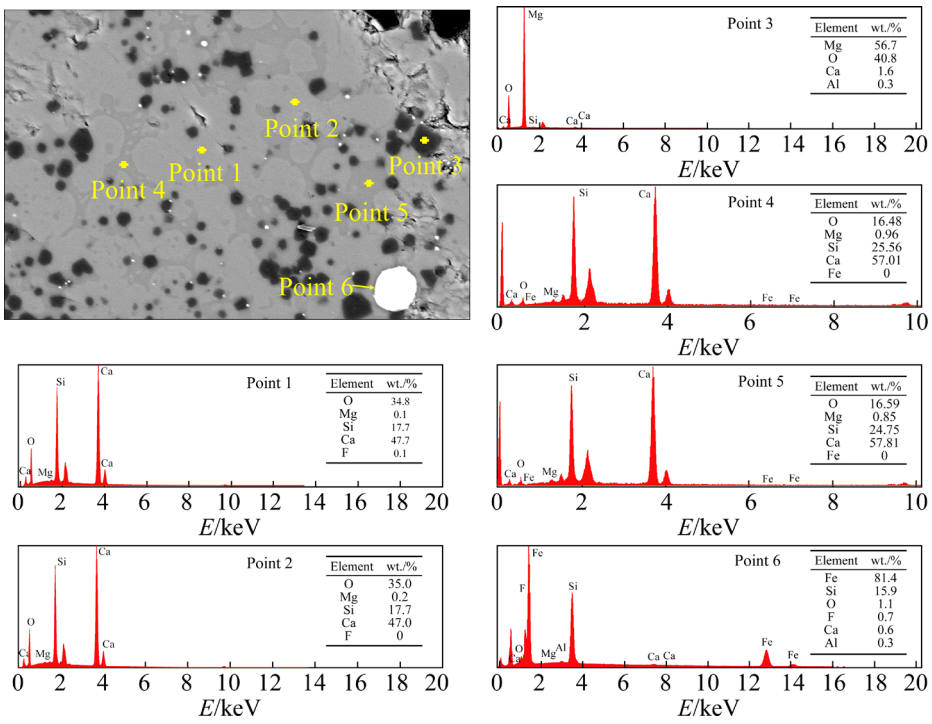

Fig. 10 Cross-sectional BSE–SEM morphology and corresponding EDS analysis results of bonded slag pellets

the bright area. Based on the EDS results and the distribution of elements, the black area is identified as MgO and the bright area comprises ferrosilicon particles. For Areas *A* and *B*, the main component of Area *A* is presumed to be Ca_2SiO_4, whereas Area *B* predominantly contains $CaSi_2$ along with some CaO.

3.5 Comparative experiment results

The reaction was performed using the initial pellets at a lower pressure as well as in an environment exceeding the calculated equilibrium pressure depicted in Fig. 6 to validate the formation conditions of the bonded slag pellets. Table 4 shows the experimental conditions and pellet conversion parameters. Under lower pressure conditions, the conversion rate of the slag pellets (referred to as Sample 1) reaches 78%. However, under conditions surpassing the calculated equilibrium pressure, the slag pellets (designated as Sample 2) exhibit a lower conversion rate, similar to that of the bonded slag pellets. The TG and DSC curves of Samples 1 and 2 are plotted in Fig. 11. Below 1200 °C, no mass loss is evident in the TG curve of Sample 1, and its DSC curve similarly shows no heat absorption peaks. However, the DSC curve of Sample 2 exhibits an endothermic peak at 1029 °C with no mass loss,

Table 4 Parameters of experimental conditions and conversion rate of Mg

Sample	Temperature/ °C	Time/ min	Pressure/ Pa	Conversion rate/%
1	1120	50	10	78
2	1120	50	40000	18

closely mirroring the bonded slag pellet results. This observation can be attributed to the solid–liquid transition of $CaSi_2$.

Moreover, the distribution regions of Mg and Ca overlap in the dolime in the form of CaO·MgO [35], which is considerably different from the separation of Mg and Ca in the bonded slag pellets.

The macromorphology of Sample 1, depicted in Fig. 12, demonstrates that the slag pellets undergo pulverization. Correspondingly, its XRD results (Fig. 12(c)) reveal pronounced peaks of γ-Ca_2SiO_4, CaO, and MgO as well as weak peaks of β-Ca_2SiO_4. However, the macromorphology of Sample 2 (Fig. 12(f)) displays that the pellets do not experience pulverization similar to the bonded slag pellets. Notably, the two pellets in Sample 2 are fused together and exhibit flexibility. Additionally, the XRD results (Fig. 12(g)) display distinct peaks of β-Ca_2SiO_4, MgO, $CaSi_2$, and CaO but lack peaks

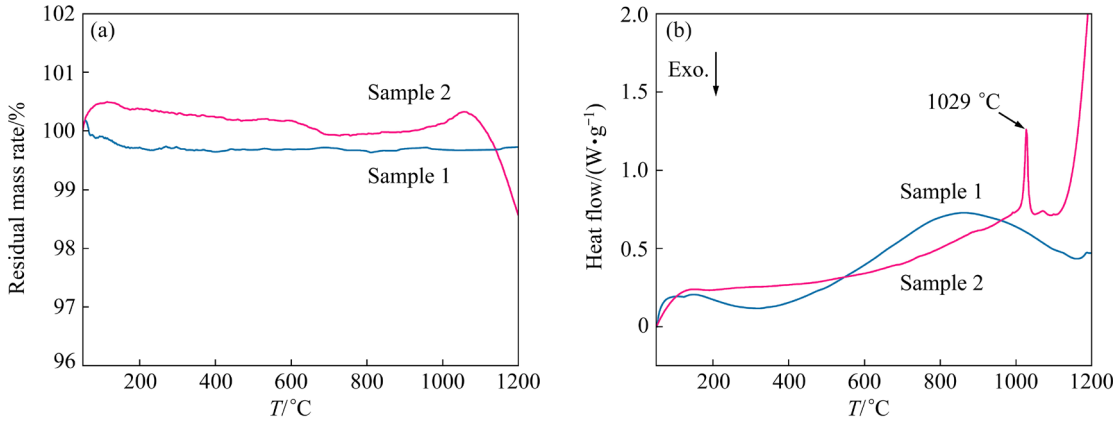

Fig. 11 TG (a) and DSC (b) curves of Samples 1 and 2

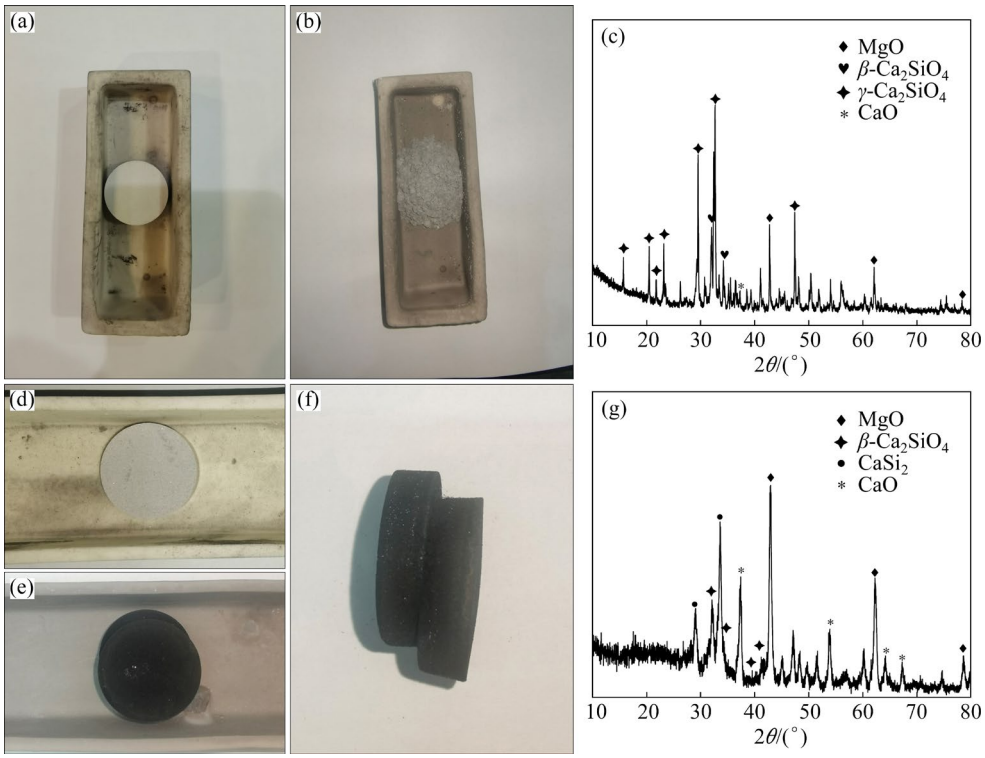

Fig. 12 Characteristics of Samples 1 and 2: (a) Macromorphology of Sample 1 before reaction; (b) Macromorphology of Sample 1 after reaction; (c) XRD pattern of Sample 1 after reaction; (d) Macromorphology of Sample 2 before reaction; (e) Macromorphology of Sample 2 after reaction; (f) Macromorphology of cross-section of Sample 2; (g) XRD pattern of cross-section of Sample 2

of γ-Ca_2SiO_4 and Si [22]. This absence suggests the non-occurrence of the crystal transition from β-Ca_2SiO_4 to γ-Ca_2SiO_4, accounting for the lack of natural pulverization in Sample 2 [25]. These findings indicate that the bonding between the pellets results from the presence of a certain amount of $CaSi_2$.

The high-magnification BSE–SEM morphology and the corresponding EPMA analysis results of Sample 2 are presented in Fig. 13. The black regions, enriched in Mg and O but devoid of Ca and Si, indicate the distribution of MgO. Excluding these black areas, the primary distribution involves Ca, O, and Si elements, with the main components presumed to be Ca_2SiO_4, $CaSi_2$, and some CaO. The micromorphology and elemental distributions closely resemble those of the bonded slag pellets. The analyses of Sample 2 suggest that if the actual pressure exceeds the theoretical equilibrium pressure or if the temperature is lower than the theoretical initial reaction temperature, Reaction (4) will be impeded.

3.6 Formation mechanism of bonded slag pellets

The aforementioned analyses are presented comprehensively in a schematic diagram (Fig. 14), elucidating the formation mechanism of bonded slag pellets in primary magnesium production via the Pidgeon process. In the standard Pidgeon process for primary magnesium production, Si initially reacts with CaO in dolime to form $CaSi_2$, as expressed in Reaction (2), simultaneously liberating free MgO. Subsequently, the liquid silicocalcium

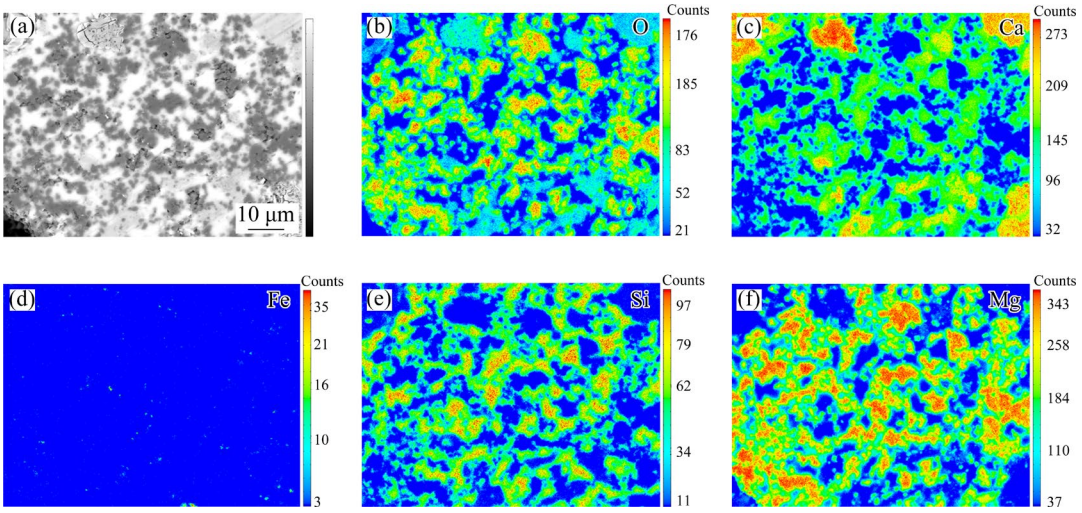

Fig. 13 High-magnification cross-sectional BSE–SEM morphology (a) and corresponding EPMA results (b−f) of Sample 2

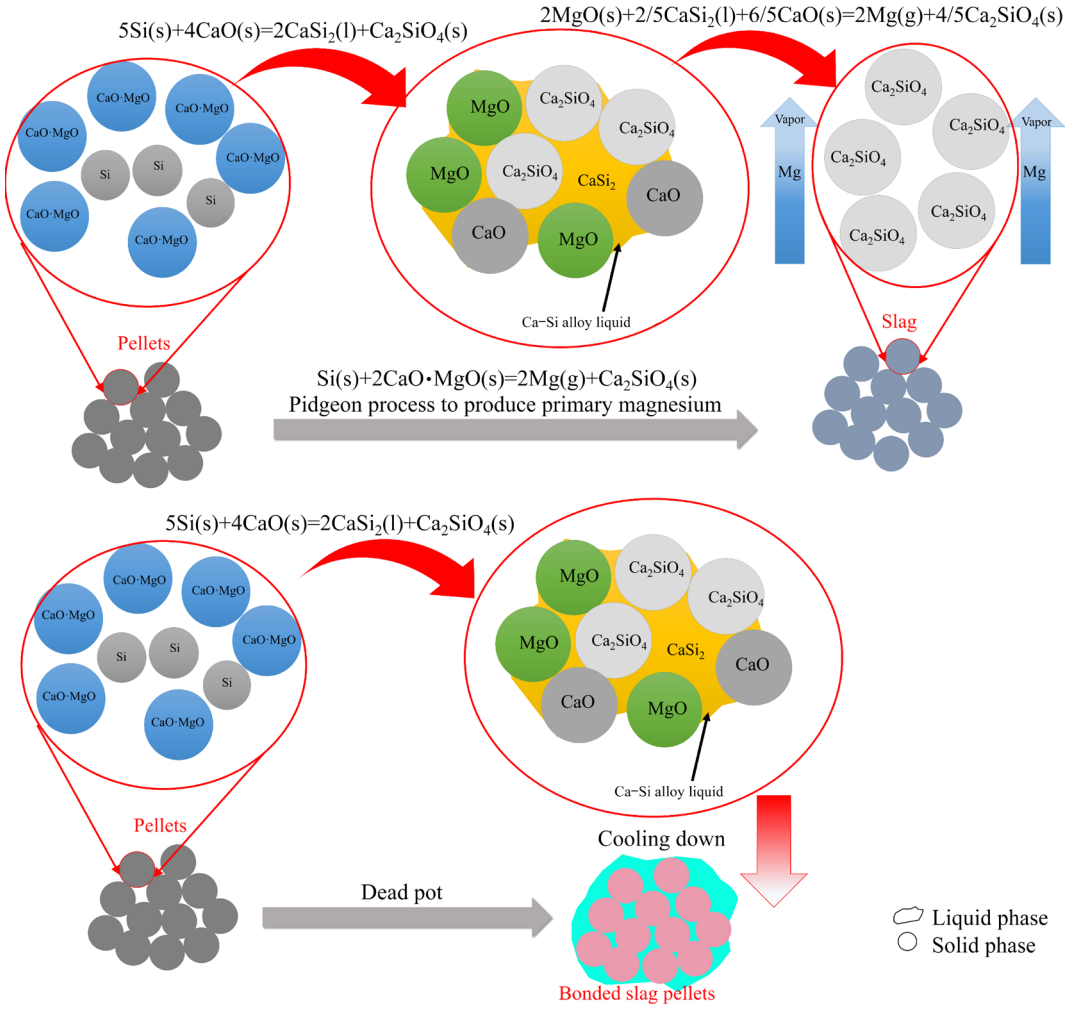

Fig. 14 Schematic diagram of formation mechanism of bonded slag pellets

alloy reduces MgO under vacuum conditions to produce magnesium vapor and Ca_2SiO_4 according to Reaction (4).

The occurrence of "dead pot" in the vertical-pot Pidgeon process can be attributed to two key factors: (1) The slag outlet, situated at the bottom of the vertical pot near the cooling jacket, potentially creates "low temperature" zones at the base of the pot; (2) Given that the crystallizer is typically positioned at the top of the vertical pot and linked to vacuum equipment, the pressure at the bottom of the pot is likely to be higher than that at the top. Additionally, any leakage in the sealing device at the bottom of the pot during the reduction stage may further elevate the bottom pressure. This combination of temperature and pressure effectively suppresses Reaction (4) in the pellets at the bottom of the pot.

To prevent the formation of bonded slag pellets, adopting appropriate measures is imperative. The temperature and pressure in the reduction pot should be maintained to avoid conditions that inhibit Reaction (4). Based on the lowest temperature in the reduction pot, the pressure should remain below the equilibrium pressure of Reaction (4) at this temperature, as depicted in Fig. 6. For instance, if the minimum temperature is 1100 °C, the pressure should be kept under 1165 Pa. Under these conditions, Reaction (4) progresses rapidly and smoothly, not only preventing the excessive build-up of liquid silicocalcium in the pellets, which leads to the formation of bonded slag pellets, but also enhancing the conversion of MgO.

4 Conclusions

(1) During magnesium production via the Pidgeon process, the actual sequence of the chemical reactions involves Si initially reducing CaO to form $CaSi_2$. Subsequently, $CaSi_2$ reacts with MgO to produce Mg vapor.

(2) The principal constituents of the bonded slag pellets are MgO, $CaSi_2$, CaO, and Ca_2SiO_4. The formation mechanism of these pellets entails Si reacting with CaO·MgO to generate Ca_2SiO_4 and liquid $CaSi_2$ at elevated temperatures while concurrently releasing free MgO. The reaction between $CaSi_2$ and MgO, crucial for producing Mg vapor, is hindered. As a result, the bonding of slag pellets is due to the solid−liquid transition of $CaSi_2$, thereby impeding slag discharge.

(3) The contributions of this study greatly enhance our understanding of slag pellet bonding, with practical implications for optimizing the Pidgeon process. Future research should explore broader methods for controlling process variables.

CRediT authorship contribution statement

Ji-lei XU: Methodology, Validation, Investigation, Software, Writing − Original draft; **Jin-hui LIU:** Methodology, Validation, Writing − Review and editing; **Yu-ming ZHAO:** Validation, Writing − Review and editing; **Zhi-ping MAO** and **Wei-neng TANG:** Conceptualization, Methodology, Supervision, Writing − Review and editing; **Xiao-feng LI** and **Pei-xu YANG:** Writing − Review and editing; **Wei-dong ZHANG:** Resources; **Shao-jun ZHANG:** Methodology, Writing − Review and editing.

Declaration of competing interest

The authors declare that they have no known competing financial interests or personal relationships that could have appeared to influence the work reported in this paper.

Acknowledgments

This work was funded by the China Postdoctoral Science Foundation (No. 2020M682337).

References

[1] LI Feng, SUN Xiang, SONG Liang, KANNAN M B, ZHANG Fen, CUI Lan-yue, ZOU Yu-hong, LI Shuo-qi, LIU Cheng-bao, ZENG Rong-chang. Influence of intermetallic Al−Mn particles on in-situ steam Mg−Al−LDH coating on AZ31 magnesium alloy [J]. Transactions of Nonferrous Metals Society of China, 2022, 32: 3926−3949.

[2] DING De-yu, DU Yu-hang, TANG Mei-fang, SONG Bo, GUO Ning, ZHANG Hong-ju, GUO Sheng-feng. Corrosion and discharge behavior of Mg−Zn−Mn−Nd alloys as primary Mg−air batteries anode [J]. Transactions of Nonferrous Metals Society of China, 2023, 33: 2014−2029.

[3] WANG Jia-hao, WU Rui-zhi, FENG Jing, ZHANG Jing-huai, HOU Le-gan, LIU Mei-duo. Recent advances of electromagnetic interference shielding Mg matrix materials and their processing: A review [J]. Transactions of Nonferrous Metals Society of China, 2022, 32: 1385−1404.

[4] YANG W, QUAN G F, JI B, WAN Y F, ZHOU H, ZHENG J, YIN D D. Effect of Y content and equal channel angular pressing on the microstructure, texture and mechanical property of extruded Mg−Y alloys [J]. Journal of Magnesium and Alloys, 2022, 10: 195−208.

[5] ZHANG Kun-ming, QIN Chen, SHE Jia, JING Xue-rui, PENG Peng, TANG Ai-tao, RASHAD M, PAN Fu-sheng. Simultaneous improvement in strength and ductility of

extruded Mg alloy via novel closed forging extrusion [J]. Transactions of Nonferrous Metals Society of China, 2022, 32: 2866−2876.

[6] GUAN Kai, ZHANG Jing-huai, YANG Qiang, LI Bai-shun, WU Rui-zhi, MENG Jian. Effects of trace Ca addition on microstructure and mechanical properties of as-cast Mg−Sm−Gd-based alloy [J]. Transactions of Nonferrous Metals Society of China, 2023, 33: 46−58.

[7] PAN Hu-cheng, PAN Fu-sheng, WANG Xiao, PENG Jian, GOU Jun, SHE Jia, TANG Ai-tao. Correlation on the electrical and thermal conductivity for binary Mg−Al and Mg−Zn alloys [J]. International Journal of Thermophysics, 2013, 34: 1336−1346.

[8] LI Shu-bo, YANG Xin-yu, HOU Jiang-tao, DU Wen-bo. A review on thermal conductivity of magnesium and its alloys [J]. Journal of Magnesium and Alloys, 2020, 8: 78−90.

[9] CHE Yu-si, ZHANG Chao, SONG Jian-xun, SHANG Xiao-jia, CHEN Xi-ping, HE Ji-lin. The silicothermic reduction of magnesium in flowing argon and numerical simulation of novel technology [J]. Journal of Magnesium and Alloys, 2020, 8: 752−760.

[10] LI Hui-quan, ZHANG Wen-juan, LI Qiang, CHEN Bo. Updated CO_2 emission from Mg production by Pidgeon process: Implications for automotive application life cycle [J]. Resources, Conservation and Recycling, 2015, 100: 41−48.

[11] CHE Yu-si, MAI Geng-peng, LI Shao-long, HE Ji-lin, SONG Jian-xun, YI Jian-hong. Kinetic mechanism of magnesium production by silicothermic reduction of CaO·MgO in vacuum [J]. Transactions of Nonferrous Metals Society of China, 2020, 30: 2812−2822.

[12] XU Jing-zhong, ZHANG Ting-an, LI Xiao-long. Research on the process, energy consumption and carbon emissions of different magnesium refining processes [J]. Materials, 2023, 16(9): 3340.

[13] LI Rong-bin, ZHANG Chao, ZHANG Shao-jun, GUO Lie-jin. Experimental and numerical modeling studies on production of Mg by vacuum silicothermic reduction of CaO·MgO [J]. Metallurgical and Materials Transactions B, 2014, 45: 236−250.

[14] WANG Chao, ZHANG Shao-jun, GUO Lie-jin. Investigation on the effective thermal conductivity of typical Pidgeon process briquette with a combined model [J]. International Journal of Heat and Mass Transfer, 2017, 115: 1348−1358.

[15] TIAN Yang, WANG Li-peng, YANG Bin, DAI Yong-nian, XU Bao-qiang, WANG Fei, XIONG Neng. Comparative evaluation of energy and resource consumption for vacuum carbothermal reduction and Pidgeon process used in magnesium production [J]. Journal of Magnesium and Alloys, 2022, 10: 697−706.

[16] YU A, HU H, LI N Y. Mathematical modelling of magnesium reduction in a novel vertical Pidgeon process [J]. Modelling and Simulation in Materials Science and Engineering, 2002, 10: 413−423.

[17] XU Ji-lei, LIU Jin-hui, GUO Dong, CHEN Mao, YANG Pei-xu, LI Rong-bin, ZHANG Shao-jun. Mechanism of slag pellets sticking on the wall of reduction pot in magnesium production by Pidgeon process [J]. Journal of Magnesium and Alloys, 2024, 12: 2397−2412.

[18] HIDAYAT T, SIREGAR M Y, SANTOSO I, ZULHAN Z. The effects of reductant and additive on the magnesium extraction from calcined dolomite via metallothermic reduction under vacuum condition [J]. Vacuum, 2022, 202: 111196.

[19] TOGURI J M, PIDGEON L M. High-temperature studies of metallurgical processes. Part II: The thermal reduction of calcined dolomite with silicon [J]. CanadIan Journal of Chemistry, 1962, 40: 1769−1776.

[20] FU Da-xue, WANG Yao-wu, ZHANG Ting-an, FENG Nai-xiang. Review on the silicothermic process for primary magnesium production [J]. Metallurgical and Materials Transactions B: Process Metallurgy and Materials Processing Science, 2023, 54: 1−21.

[21] YOU Jing, WANG Yao-wu. Reduction mechanism of Pidgeon process of magnesium metal [J]. Chinese Journal of Process Engineering, 2019, 19: 560−566. (in Chinese)

[22] MORSI I M, ELBARAWY K A, MORSI M B, ABDEL-GAWAD S R. Silicothermic reduction of dolomite ore under inert atmosphere [J]. Canadian Metallurgical Quarterly, 2002, 41: 15−28.

[23] MORSI I M, ALI H H. Kinetics and mechanism of silicothermic reduction process of calcined dolomite in magnetherm reactor [J]. International Journal of Mineral Processing, 2014, 127: 37−43.

[24] FU Da-xue, JI Zong-hui, GUO Jun-hua, HAN Ji-biao, DOU Zhi-he, LIU Yan, ZHANG Ting-an, GUAN Lu-kui. Diffusion and phase transformations during the reaction between ferrosilicon and CaO·MgO under vacuum [J]. Journal of Materials Research and Technology, 2020, 9: 4379−4385.

[25] SAIDANI S, SMITH A, EL HAFIANE Y, BEN TAHAR L. Re-examination of the $\beta\rightarrow\gamma$ transformation of Ca_2SiO_4 [J]. Journal of the European Ceramic Society, 2018, 38: 4756−4767.

[26] CASTILLO S M, TANG Zhong-jia, LITVINCHUK A P, GULOY A M. Lattice dynamics of the rhombohedral polymorphs of $CaSi_2$ [J]. Inorganic Chemistry, 2016, 55: 10203−10207.

[27] YAOKAWA R, NAGOYA A, NAKANO H. Polymorphic transformations of $CaSi_2$ and $CaGe_2$ [J]. Journal of Solid State Chemistry, 2021, 295: 121919.

[28] YAOKAWA R, NAKANO H, OHASHI M. Growth of $CaSi_2$ single-phase polycrystalline ingots using the phase relationship between $CaSi_2$ and associated phases [J]. Acta Materialia, 2014, 81: 41−49.

[29] RHEINHEIMER V, CASANOVA I. An X-ray photoelectron spectroscopy study of the hydration of C_2S thin films [J]. Cement and Concrete Research, 2014, 60: 83−90.

[30] LIU Yang, FU Yong-qing, CHEN Tu-pei, TSE M S, FUNG S, HSIEH J H, YANG Xiao-hong. Depth profiling of Si oxidation states in Si-implanted SiO_2 films by X-ray photoelectron spectroscopy [J]. Japanese Journal of Applied Physics. Part 2: Letters, 2003, 42: 8−11.

[31] ZHANG Wa-li, ZHANG Sam, YANG Ming, CHEN Tu-pei. Microstructure of magnetron sputtered amorphous SiO_x films: Formation of amorphous Si core−shell nanoclusters [J]. Journal of Physical Chemistry C, 2010, 114: 2414−2420.

[32] BLACK L, STUMM A, GARBEV K, STEMMERMANN P,

HALLAM K R, ALLEN G C. X-ray photoelectron spectroscopy of the cement clinker phases tricalcium silicate and β-dicalcium silicate [J]. Cement and Concrete Research, 2003, 33: 1561−1565.

[33] DEMRI B, MUSTER D. XPS study of some calcium compounds [J]. Journal of Materials Processing Technology, 1995, 55: 311−314.

[34] WANG Yao-wu, ZHAO Kun, PENG Jian-ping, DI Yue-zhong, LI Ying-long, SONG Yang, DENG Xin-zhong. Process of producing magnesium by thermal vacuum reduction using silicocalcium as reductant [J]. Rare Metals, 2016, 35: 571−575.

[35] FU Da-xue, WANG Yao-wu, PENG Jian-ping, DI Yue-zhong, TAO Shao-hu, FENG Nai-xiang. Mechanism of extracting magenesium from mixture of calcined magnesite and calcined dolomite by vacuum aluminothermic reduction [J]. Transactions of Nonferrous Metals Society of China, 2014, 24: 2677−2686.

竖罐皮江法炼镁黏结渣球的形成机理

许记雷[1]，刘金辉[1]，赵玉明[2]，毛志平[1]，唐伟能[3]，李晓峰[3]，杨沛胥[1]，张伟东[1]，张少军[1]

1. 郑州大学 材料科学与工程学院，郑州 450001；
2. 河南工程学院 材料工程学院，郑州 451191；
3. 中国宝武钢铁集团公司 宝钢金属股份有限公司，上海 200940

摘　要：竖罐皮江法还原罐底部偶尔会出现黏结渣球的现象，导致无法顺利排渣。利用热力学计算、X 射线衍射(XRD)、X 射线荧光光谱(XRF)、电子探针显微分析仪(EPMA)、X 射线光电子能谱(XPS)和差示扫描量热法(DSC)研究了黏结渣球的形成机理。黏结渣球的主要成分是 MgO、$CaSi_2$、CaO 和 Ca_2SiO_4。黏结渣球中存在 $CaSi_2$ 是由于 Si 还原 CaO 生成了液态 $CaSi_2$。同时，$CaSi_2$ 和 MgO 之间产生 Mg 蒸气的反应被抑制，导致 $CaSi_2$ 在料球中积累。由于 $CaSi_2$ 的固液转变，这一过程最终导致渣球之间黏结。这项研究可以指导皮江法工艺优化，缓解“死罐”问题，从而提高效率并降低成本。

关键词：竖罐皮江法；排渣；黏结渣球；$CaSi_2$；固液转变

(Edited by Wei-ping CHEN)